Towards Clinical 7T MRI

Graham C. Wiggins, D Phil; Daniel K. Sodickson, MD, PhD

Center for Biomedical Imaging, Department of Radiology, New York University Langone Medical Center, New York, NY, USA

Introduction

Many researchers in the field of ultra-high-field magnetic resonance have become accustomed to bracing themselves for an oft-repeated question. This question may arise during lulls in conversation with clinical colleagues, or during interviews with interested visitors from the press or the lay public, or, more delicate still, during reviews of our applications for research funding. The question is brief, and to the point: *'When will 7 Tesla scanners be ready for clinical use?'* Each of us has his or her own variant on a standard answer to this question, citing particular populations or disease processes in which we have obtained extraordinarily promising images, and outlining the technical hurdles which are gradually falling behind us as research advances. This twofold answer actually encapsulates two distinct strains of 7T research, each of which has an important part to play in defining the eventual clinical role of 7T MR. The first involves identification of unique information available only at ultra-high field strength, enabled for example by extremely high spatial and spectral resolution or by contrast mechanisms which are enhanced as field strength increases. The potential to access this unique information helped to motivate the original development of commercial 7T scanners, and fueled a great sense of enthusiasm as the first whole-body 7T systems arrived on the scene and the first jaw-dropping images began to emerge from those systems. This initial period of exuberant discovery was followed by an equally fascinating but also laborious period of extended basic development, during which 7T research teams began to grapple with the fact that not only the potential information content but also the routine operations of 7T scanners differed from what we had come to expect with lower-field scanners. Coils and pulse sequences required careful redesign and optimization, artifacts only hinted at in low-field settings became critical determinants of image quality at 7T, and new constraints on sequence types and parameters changed both the workflow and the content of day-to-day imaging protocols. In the past several years, a growing cadre of high-field researchers has risen to these challenges, seeking to identify the novel RF structures, calibration procedures, and spin manipulations that can eke the best performance out of 7T scanners. The goal of this second strain of research, occurring in parallel with the first, is to replicate some of the breadth and routine image quality of low-field scans, overcoming any and all practical obstacles along the way. Such nominally replicative research has actually spurred a remarkable range of technological and methodological innovation: witness the rise of parallel transmission techniques, reported in previous editions of this magazine, which have become a common component in many 7T research programs but which have already begun to have an impact on lower field strengths. Perhaps of equal importance, however, is the fact that research aimed at achieving high image quality across multiple examination types and body regions addresses an important requirement for what might be considered an ideal clinical 7T imaging platform: the ability to provide unique clinically-relevant information for a variety of disease processes without sacrificing traditional clinical image content in routine examinations. A 7T scanner with this ability need not be relegated to research tool or niche diagnostic device, but can take its place as a valuable component of the day-to-day clinical arsenal. This article reports on recent developments in the twofold pursuit of unique information content and routine usability at 7T, drawing examples from imaging experience at our institution. The clinical transformation of 7T scanning is by no means complete, but the picture that has begun to emerge is striking.

Unique clinical potential: A gallery of pathology-targeted 7T images from toe to head

The principal advantages of ultra-high field strength for MR imaging are **a)** increased signal-to-noise-ratio (SNR), which can be used to increase spatial resolution, to shorten scan time, and/or to enable imaging of low-sensitivity nuclei other than hydrogen; and **b)** enhanced contrast mechanisms such as those based on susceptibility-related effects. The corresponding challenges associated with 7T MRI include increased inhomogeneity of the RF transmit and the B_0 fields (which result in increased artifacts in various classes of pulse sequence) and increased RF energy deposition into tissue, as quantified by specific absorption rate (SAR), which can limit the range of sequence parameters which may safely be employed. 7T MRI of the brain has now become fairly routine, with the availability of reliable high-performance head coils, and high quality images in a variety of contrasts can be obtained. We will demonstrate later

1 The NYU 7 Tesla scanner.

2 Sagittal image of the ankle of a healthy adult subject. Note high-resolution depiction of cartilage and trabecular bone. (Fat-suppressed 3D FLASH, 0.23 x 0.23 x 1 mm^3, TR/TE 26/5.1 ms, 60 partitions, acquisition time 6:58 min, custom-designed transmit-receive extremity coil array with 8 receive elements.)

how a standard 3T clinical neuro imaging protocol can be translated to 7T, illustrating both advantages and challenges of ultra-high-field imaging, and presenting the opportunity to obtain familiar image contrasts while also exploring higher resolution and new contrast mechanisms in a single 7T scan session. The musculoskeletal system has become another highly fruitful area of 7T application, and we begin our catalogue of images there, proceeding from foot to head. Body imaging at 7T (e.g. targeting the heart, abdomen, or pelvis) continues to present unique challenges at 7T. However, 7T body imaging has been the subject of intensive recent attention, with striking examples provided and creative approaches undertaken by various ultra-high-field research groups. As mentioned earlier, parallel transmission and other related methods are currently under investigation to mitigate the particularly substantial B_1 inhomogeneities observed over large fields-of-view in the torso, and also to control SAR. Meanwhile robust imaging of selected body areas such as the breast may already be obtained at 7T with conventional single channel excitation.

At our institution, the past year or two has seen a surge of clinical interest in our 7T scanner, as clinical colleagues in our Department of Radiology and elsewhere have partnered with our basic researchers to probe anatomical details and pathologic processes for which key information has proven to be elusive at lower field strength. The backlog and hours of use of our 7T system have both increased markedly, and it has become an increasingly commonplace occurrence to find a radiologist at the console. The images that follow, all obtained on the Siemens MAGNETOM whole-body 7T scanner at the Center for Biomedical Imaging at NYU School of Medicine (Fig. 1), illustrate some of the multifaceted clinical promise of 7T MRI. These images, which we have sorted by body region and, when appropriate, disease process, are intended to indicate the image quality which may now be achieved at 7T with modern RF coil arrays and pulse sequences. The examples shown here represent only a subset of *in vivo* 7T scans at our center, and an even smaller subset of the work being done at a growing number of Siemens 7T sites around the world.

Ankle

Figure 2 shows a sagittal image of the ankle obtained at 0.23 x 0.23 mm^2 in-plane resolution in a healthy adult subject using a custom-designed transmit-receive extremity coil array [1]. Note the high-resolution depiction both of cartilage and of trabecular bone in this image. Although no particular pathology is evident in this example, the ability to resolve cartilage and bone structure at this level becomes a powerful asset for the detection and characterization of disease processes like those in the examples to follow.

Knee

Osteoarthritis

Figures 3 and 4 compare 7T scans of healthy adult subjects with corresponding scans of patients with radiographically documented osteoarthritis. Each of these images was obtained using a 28-element 7T knee coil array developed by Quality Electrodynamics (QED), LLC [2] and expected to be available com-

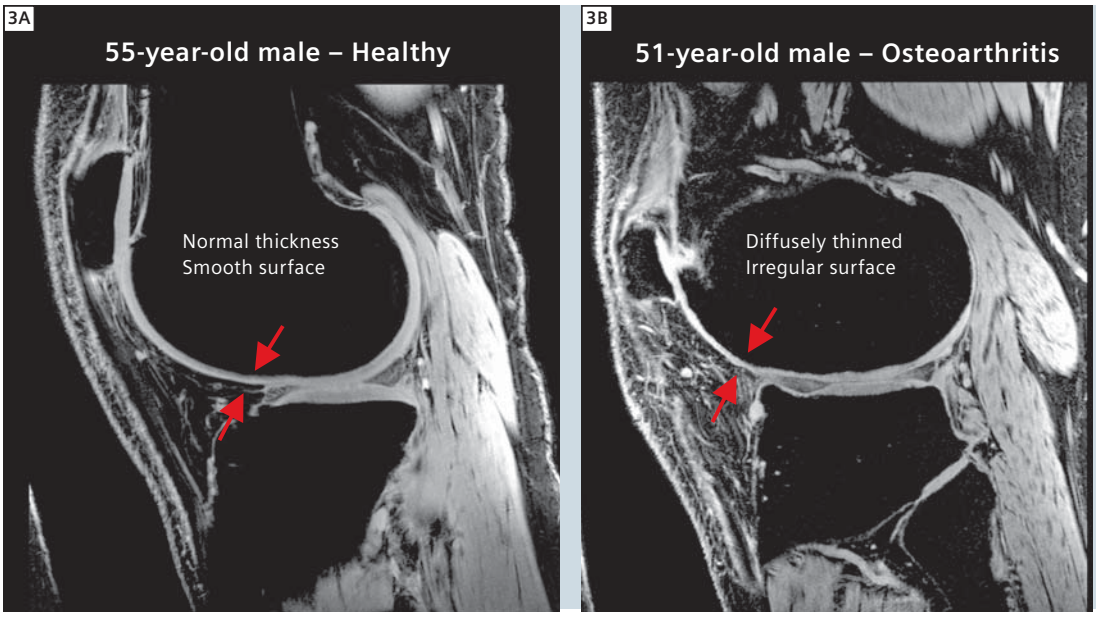

3 The high spatial resolution available at 7T enables visualization of the diffusely thinned irregular cartilage surface in a patient with osteoarthritis (right), as compared with an age-matched healthy subject (left). (Fat-suppressed 3D FLASH, TR/TE 26/5.1 ms, 0.23 x 0.23 x 1 mm³, 60 partitions, acquisition time 6:58 min, transmit-receive 7T knee coil array with 28 receive elements from QED. *Images courtesy of Gregory Chang, M.D., Department of Radiology, NYULMC, USA).*

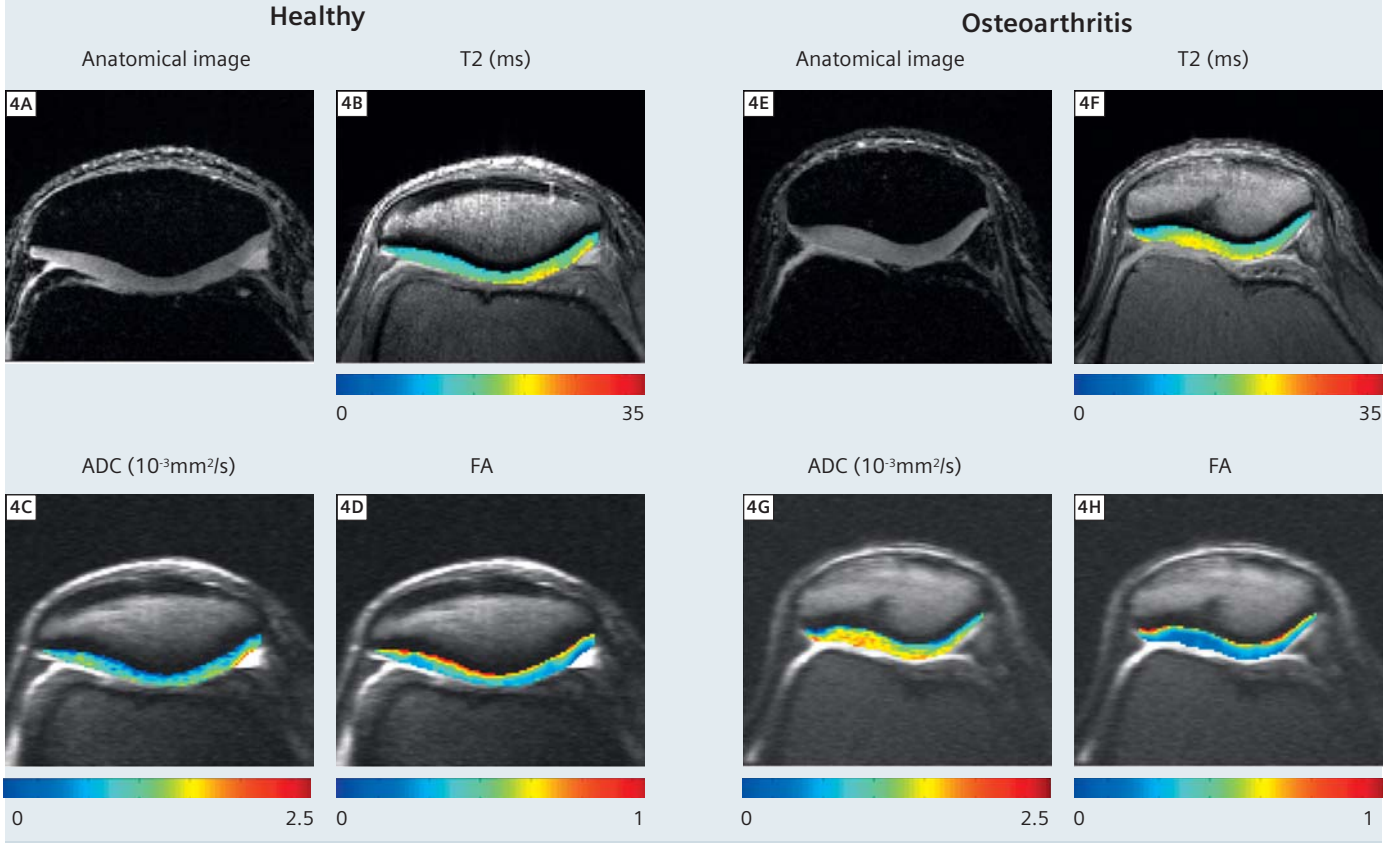

4 Apparent diffusion constant (ADC) and fractional anisotropy (FA) maps derived from line-scan diffusion acquisitions (bottom row) juxtaposed to anatomical images and T_2 maps in the knees of a healthy adult subject (left) and a patient with osteoarthritis (right). Increased ADC and decreased FA are seen in diseased tissue, reflecting microscopic changes in the fiber structure of the cartilage. (Line Scan Diffusion Tensor Imaging sequence: TE/TR/TReff 46/180/2890 ms, 0.6 x 0.6 x 2 mm³, 5 slices, b-values 5, 450 s/mm², 6 directions, fat-saturation, acquisition time 14:00 min; Anatomical images: T_2*-weighted fat-saturated GRE, TE/TR 9.2/40 ms, 0.5 x 0.5 x 0.5 mm², acquisition time 10:00 min; T_2-mapping acquisitions: multi-slice 2D multi-echo fat-saturated sequence with stimulated echo suppression, TE/TR 16/3500 ms, 0.6 x 0.6 x 2 mm³, 5 slices, echo train length 8, acquisition time 13:35 min. QED 28-element 7T knee array used in all cases. *Images courtesy of Jose Raya, Ph.D., NYULMC, USA.*)

mercially in the near future. The 0.23 x 0.23 mm^2 in-plane spatial resolution of the sagittal images in Figure 3 is sufficient for direct visual appreciation of the diffusely thinned and irregular cartilage surface in the osteoarthritic patient. The images in Figure 4, on the other hand, are targeted to microscopic changes in cartilage structure and function. In addition to anatomical images and T_2 maps, maps of apparent diffusion constant (ADC) and fractional anistropy (FA) are shown, derived from line-scan diffusion acquisitions. The decreased FA in the cartilage of subjects with osteoarthritis is consistent with structural damage to the collagen network. The increased ADC, on the other hand, may be shown to result from reduced proteoglycan content. Figure 5 illustrates the potential value of 7T scanning for a complementary evaluation of proteoglycan content, and therefore of cartilage function. These images represent various slices through 3D volumetric sodium concentration maps encompassing the whole knee in a healthy subject as compared with a patient with osteoarthritis (OA). The enhanced SNR available at 7T enabled whole-knee acquisitions at 2 mm isotropic resolution in less than 15 minutes. Such acquisitions would not be possible at lower field strengths, given inherently low MR sensitivity to sodium nuclei. Through appropriate calibration, sodium images were converted into quantitative sodium concentrations, which may be seen to be generally decreased in the osteoarthritic as compared with the healthy knee cartilage. Indeed, the average sodium concentration across the knee cartilage in 5 patients with OA was noticeably lower than that in a group of 5 healthy controls. This change reflects a loss of proteoglycans, the removal of whose net negative charge results in a corresponding loss of positively-charged sodium ions to preserve charge balance.

Healthy subject (average [Na] ~ 240-280 mM in 5 healthy subjects)

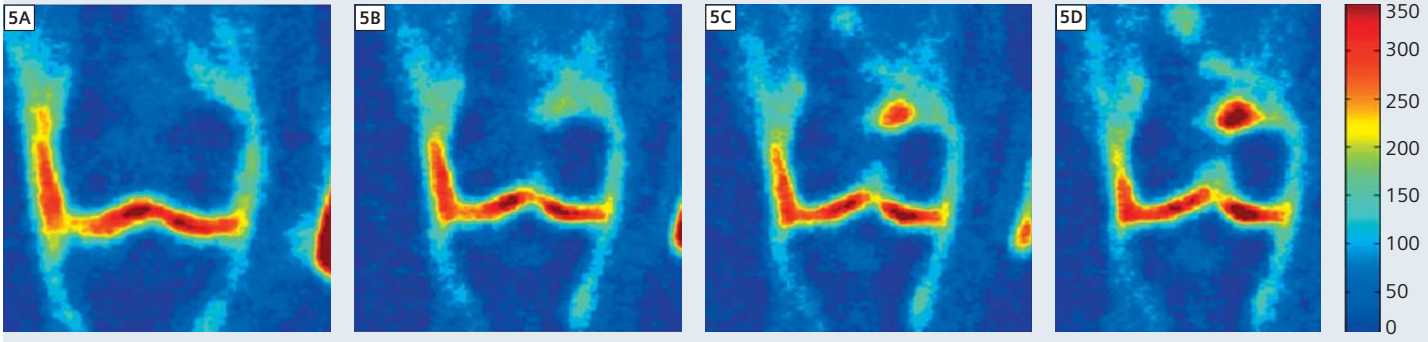

Patient with OA (average [Na] ~ 180-240 mM in 5 patients)

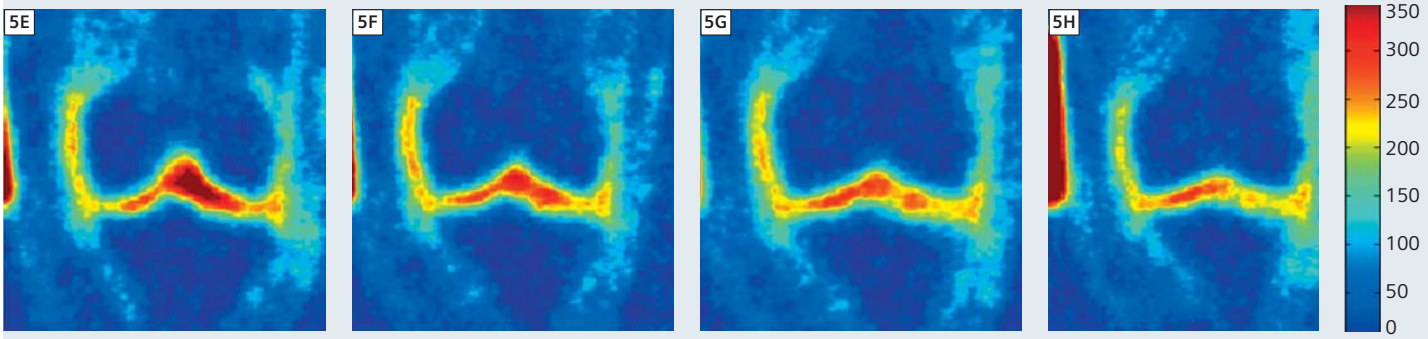

5 7T sodium imaging of cartilage in a healthy subject (top) and a patient with osteoarthritis (bottom). 7T field strength enabled whole-knee 3D volumetric sodium concentration maps at comparatively high resolution in less than 15 minutes. Note reductions in average sodium concentration in arthritic versus healthy cartilage, both in the individual knees shown and in ensembles of 5 patients and 5 controls. (Undersampled 3D radial pulse sequence, TR/TE 80/0.2 ms, 2.0 x 2.0 x 2.0 mm^3, single-tuned quadrature sodium coil custom-designed in collaboration with Rapid Biomedical, GmbH. *Images courtesy of Ravi Regatte, Ph.D., Department of Radiology, NYULMC, USA.*)

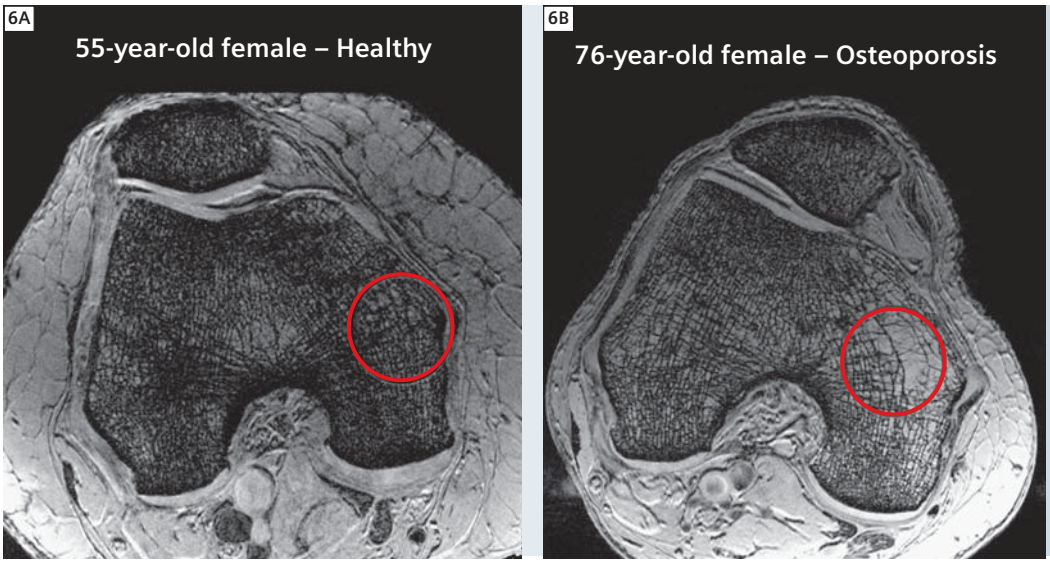

6 Images of the distal femur of a healthy subject (left) and a patient with osteoporosis (right). Note the reduction in density of trabecular bone structure in the patient as compared with the control (for example, in the circled regions of interest). (3D FLASH, TR/TE 20/5.1ms, 0.23 x 0.23 x 1.0 mm^3, 80 partitions, acquisition time 7:09 min, QED 28-element knee coil array. *Images courtesy of Gregory Chang, M.D., Department of Radiology, NYULMC, USA.*)

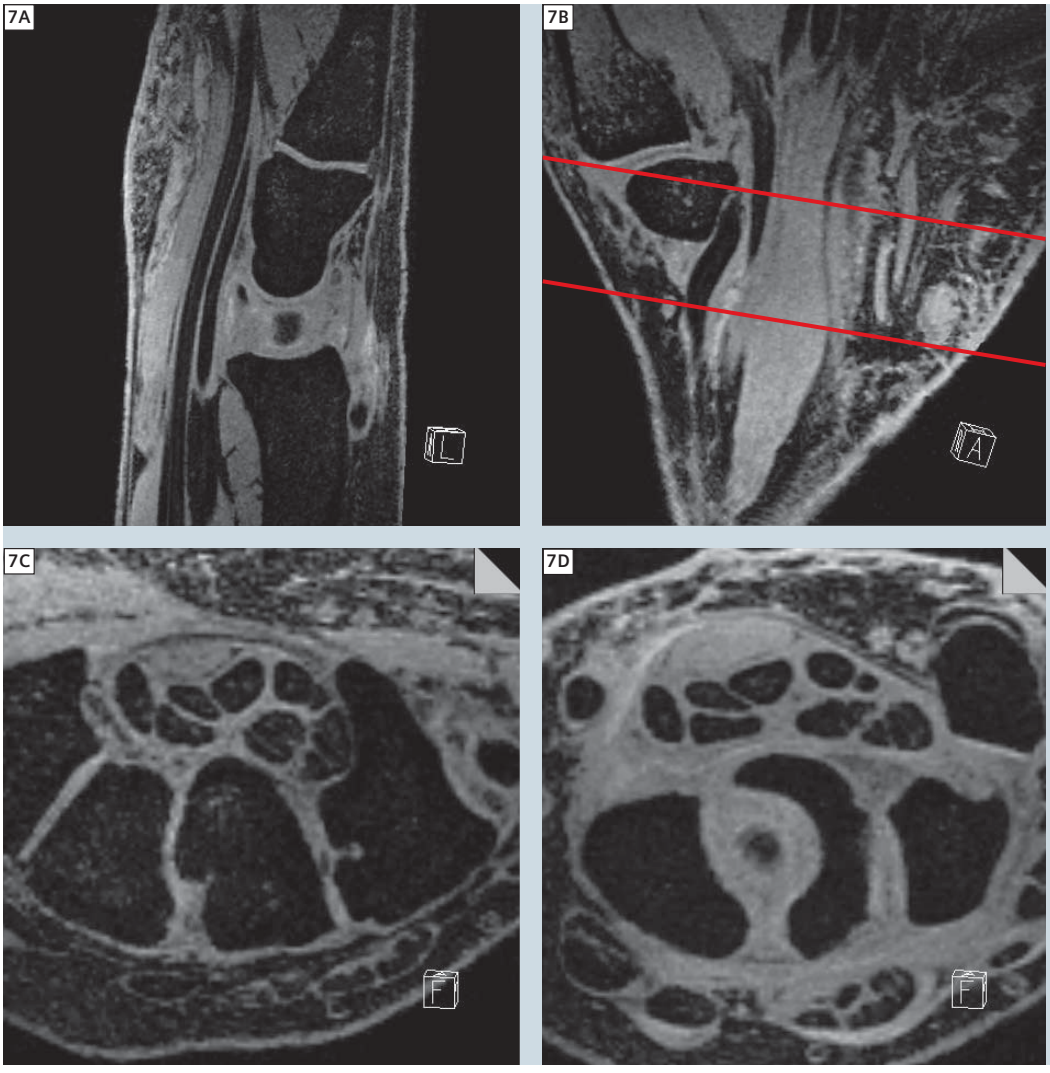

7 Images from a 0.33 mm^3 isotropic 3D gradient-echo acquisition in a patient with Carpal Tunnel Syndrome. The red lines in the top right image indicate the image plane geometry of the bottom two images. The anatomy within the carpal tunnel is clearly delineated, and pronounced swelling of the median nerve may be appreciated. (3D FLASH, TR/TE 40/3.2 ms, 0.33 x 0.33 x 0.33 mm^3, 128 partitions, acquisition time 7:10 min, custom-built 8-element 7T extremity coil array. *Images obtained as part of a collaboration with Dr. David Chiu, Department of Surgery, NYULMC, USA.*)

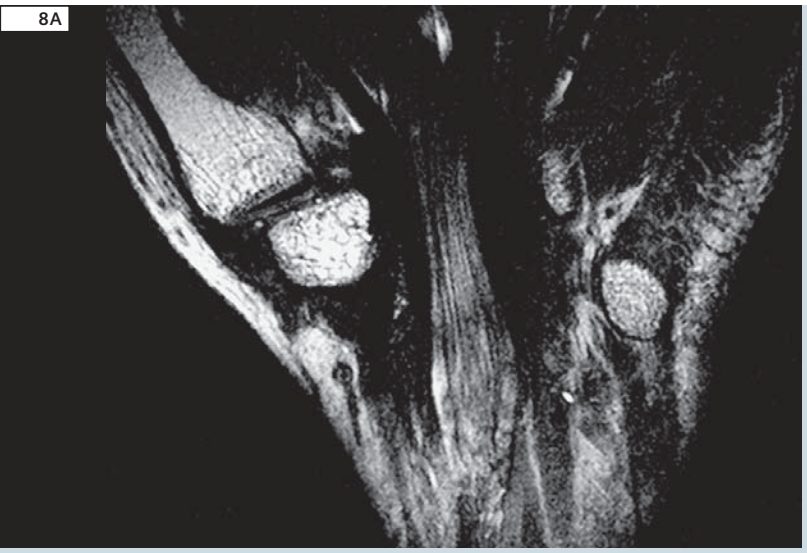

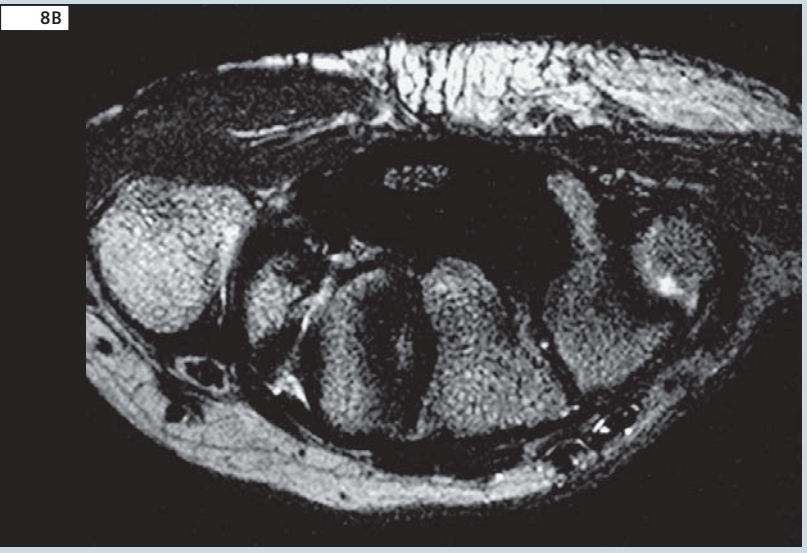

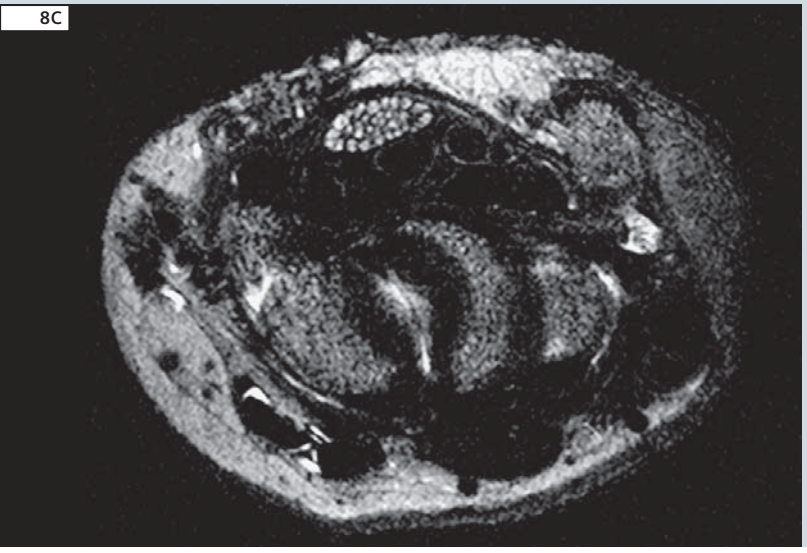

8 2D spin-echo images of a patient with Carpal Tunnel Syndrome. Individual fascicles of the inflamed median nerve can be tracked even through the constriction at the carpal tunnel. (2D TSE, TR/TE 5500/87 ms, 0.2 x 0.2 x 1 mm³, 13 slices, Turbo Factor 13, acqui-sition time 3:35 min, custom-built 8-element 7T extremity coil array. *Images obtained as part of a collaboration with Dr. David Chiu, Department of Surgery, NYULMC, USA.*)

Osteoporosis

In Figure 6, osteoporotic changes in trabecular bone structure may be appreciated directly from axial 7T images, rather than being probed indirectly through projection-based densitometry. This enables assessment not only of bone density but also of bone quality [3, 4]. The image of the osteoporotic patient shows fewer and more widely-separated dark trabeculae with larger marrow spaces between them. This structure reflects a reduced bone strength and a correspondingly increased fracture risk. In fact, it is believed that bone density alone accounts for only 50–60% of the fracture risk in osteoporotic patients, with the remaining risk attributable to bone quality [3]. Thus, 7T imaging has the potential to improve our ability to assess bone strength and clinical fracture risk.

Wrist

Carpal Tunnel Syndrome

In collaboration with interested surgeons at our institution, we have begun to study patients with Carpal Tunnel Syndrome at 7T. The resulting high-resolution depiction of structures surrounding and running through the carpal tunnel, as exemplified in Figures 7 and 8, will enable definitive diagnosis, as well as helping to define surgical approaches and allowing the creation of detailed anatomical atlases in the presence and the absence of pathology.

9 Sagittal 7T images (left, full field-of-view; right, close-up of boxed area) of the spine of a 19 year-old male with a cavernous angioma at T5 discovered incidentally on earlier lower-field MR scans. Imaging at 7T improved spatial resolution and lesion visualization as compared with 1.5T and 3T scans, though certain details are still obscured by susceptibility artifacts from residual blood products. (2D TSE 0.55 x 0.55 x 1.5 mm³, TR/TE 6000/10 ms, 11 slices, acquisition time 4:55 min, custom-built transmit-receive 7T spine array with 8 receive elements.)

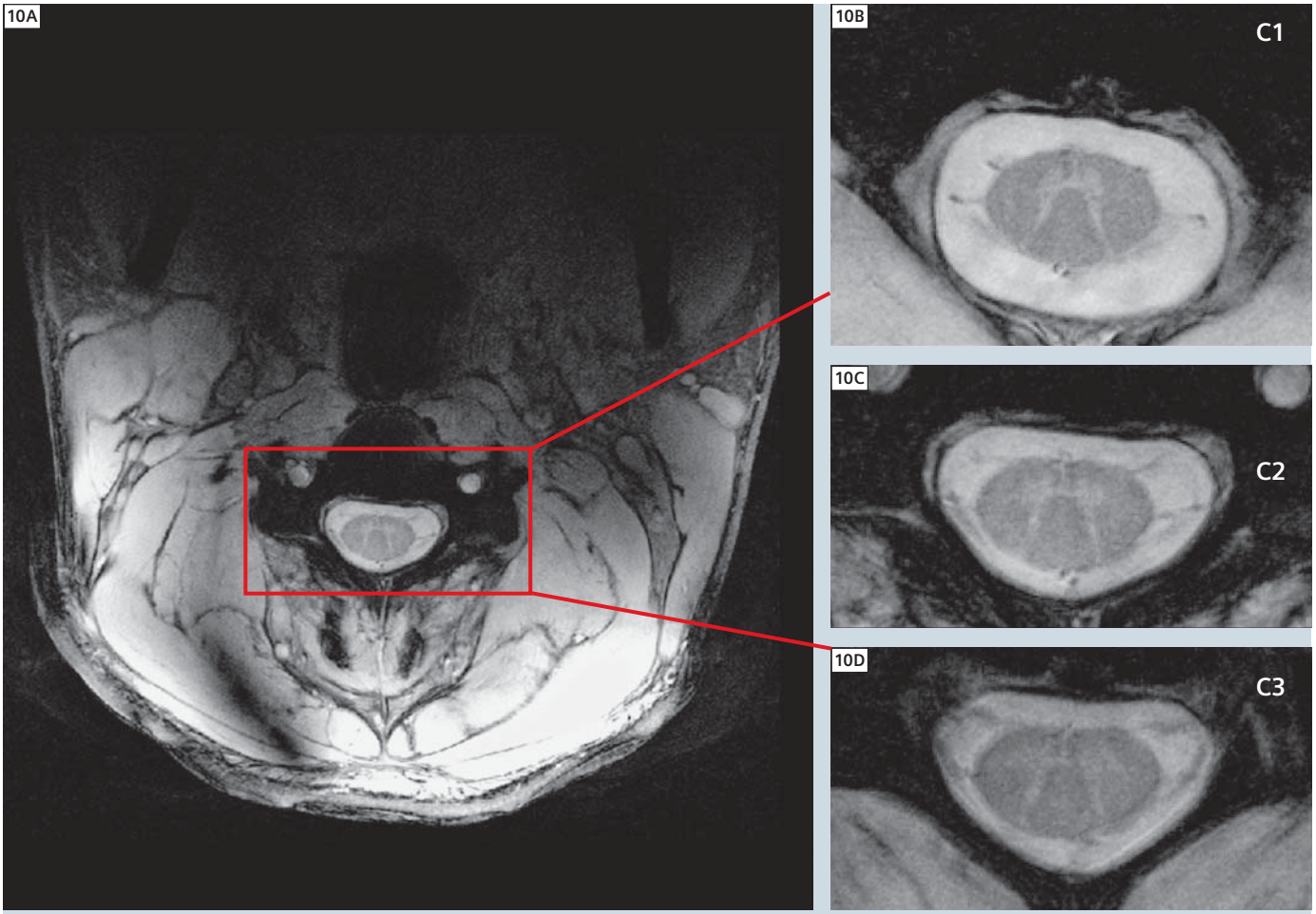

10 High spatial resolution enables noninvasive visualization of spinal cord structure with unprecedented detail. (2D gradient echo, 0.18 x 0.18 x 3.0 mm³, TR/TE 500/4.91 ms, 5 slices, 4 element transmit-receive C-spine array from Rapid Biomedical GmbH. *Images courtesy of Eric Sigmund, Ph.D., Department of Radiology, NYULMC, USA.*)

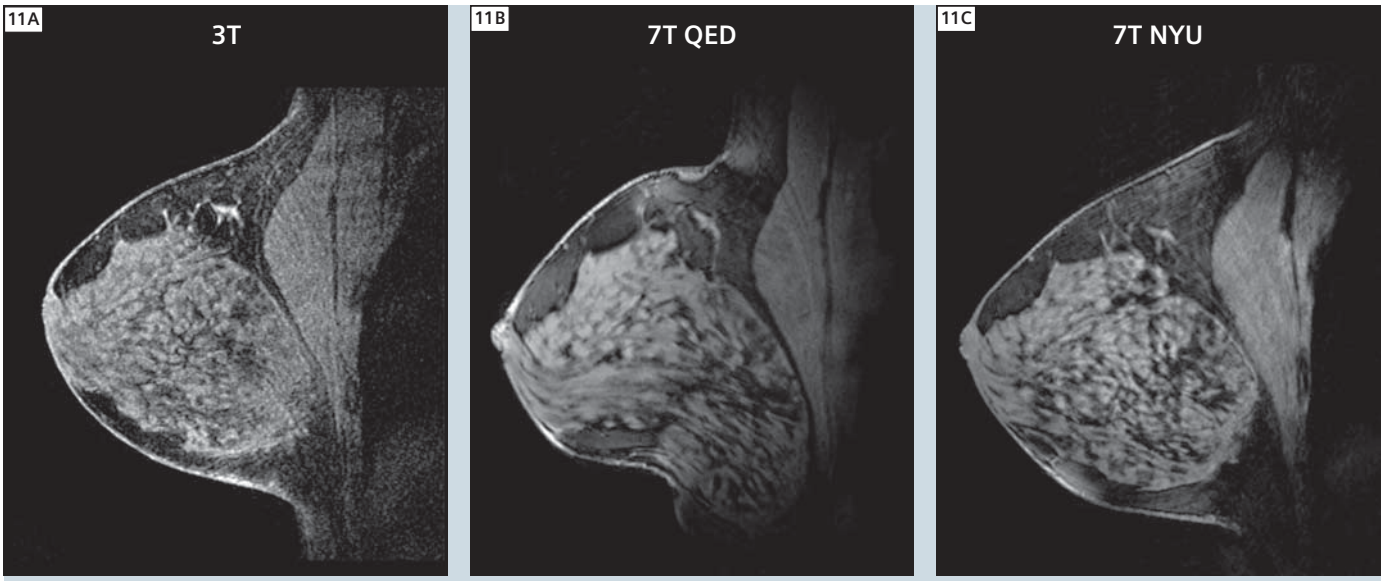

11 Comparison of 3T (left, In Vivo Corp. 4-element receive coil array) and 7T breast images (middle: QED 16-element coil array; right: NYU custom-designed 2-element coil array). 7T images have significantly higher SNR for the same image resolution and total acquisition time. (3D GRE with Fat Saturation, TR/TE 4.37/1.92 ms, 0.6 x 0.6 x 0.6 mm^3, 208 partitions, acquisition time 4:28 min. *Images courtesy of Ryan Brown, Ph.D., NYULMC, USA.*)

Thoracic Spine
Cavernoma

Figure 9 documents the case of a 19-year-old patient whose cavernous angioma at thoracic spinal level T5 was discovered incidentally on a 1.5T MR scan at another institution following a sporting accident. Subsequent 3T imaging was also performed in an attempt to determine the feasibility and advisability of surgery for this otherwise asymptomatic young man, but image quality was insufficient to define the detailed internal structure of the lesion and the surrounding spinal cord. The family came to our center in the hope that 7T imaging could further inform their decision and guide a potential surgical approach. A team of physicists, RF engineers, technologists, neuroradiologists, and spinal surgeons was mobilized to address this challenging question. Figure 9 shows sagittal images at two magnifications highlighting the lesion. Using a custom-built 8-channel transmit-receive 7T spine array [5] and optimized gradient-echo and spin-echo pulse sequences, nearby cord structure could be defined with unprecedented detail. Unfortunately, residual blood products in the vascular lesion resulted in susceptibility-related signal voids in the immediate vicinity of the lesion, preventing ideal delineation. Work is now underway to apply susceptibility-insensitive approaches for further improved visualization. This example highlights both the promise and some of the ongoing practical challenges associated with clinical 7T studies.

Cervical Spine

Figure 10, on the other hand, shows the exquisite delineation of spinal cord substructure which may be achieved at 7T in regions not subject to high susceptibility gradients. In these images, obtained with a 4-element transmit-receive C-spine coil array from Rapid Biomedical, GmbH, excellent spatial detail is observed, differentiating gray/white matter tissue, dorsal and ventral nerve roots, denticulate ligaments, dura mater, pia mater, and rostral-caudal blood vessels.

Breast

Figure 11 compares breast images obtained in the same healthy adult subject at 3T and at 7T. Substantial increases in SNR are evident for the same spatial resolution and total acquisition time in the 7T images. 3T images were acquired using a commercially-available 4-element receive-only 3T breast array from In Vivo Corp. 7T images were acquired both with a commercial transmit-receive breast coil array with 16 receive elements from QED and with a custom-designed 2-element transmit-receive breast array developed at our Center. Our custom-designed 7T coil array has also been used to characterize the distribution of T_1 and T_2 values and B_0 field distribution in healthy breast tissue [6], in preparation for clinical studies to come. Some further development and pulse sequence optimization is called for to reap the full benefits of 7T SNR enhancements, but 7T imaging may be expected to shift favorably the balance of spatial and temporal resolution which is so crucial for characterization of breast cancer.

Brain

For neurological applications, the high intrinsic SNR and the correspondingly high achievable spatial resolution at 7T may be used to resolve brain structures which have until now eluded direct visualization with MR. Susceptibility- or T_2*-weighted images in particular can provide extraordinarily high levels of anatomical detail, in addition to affording striking tissue contrast, some of whose precise physical sources are still being investigated. At NYU we have begun to scan volunteers with a variety of known brain diseases to begin exploring what new clinically- and biologically-relevant information may be found at 7T.

Tuberous sclerosis

Recently, a collaboration has arisen between basic researchers, pediatric neuroradiologists, pediatric neurosurgeons, and epileptologists at our institution, aimed at investigating the biological substrate of tuberous sclerosis, a group of genetic disorders with a spectrum of symptoms including potentially intractable seizures. Figure 12 shows images from a patient with tuberous sclerosis. This patient was imaged first with a high resolution T_1-weighted MPRAGE sequence and then with a 3D FLAIR sequence. The high isotropic spatial resolution of these images allows visualization not only of tubers (like the one indicated by red arrows in the figure), but also of subtle signs of cortical dysplasia (blue arrow).

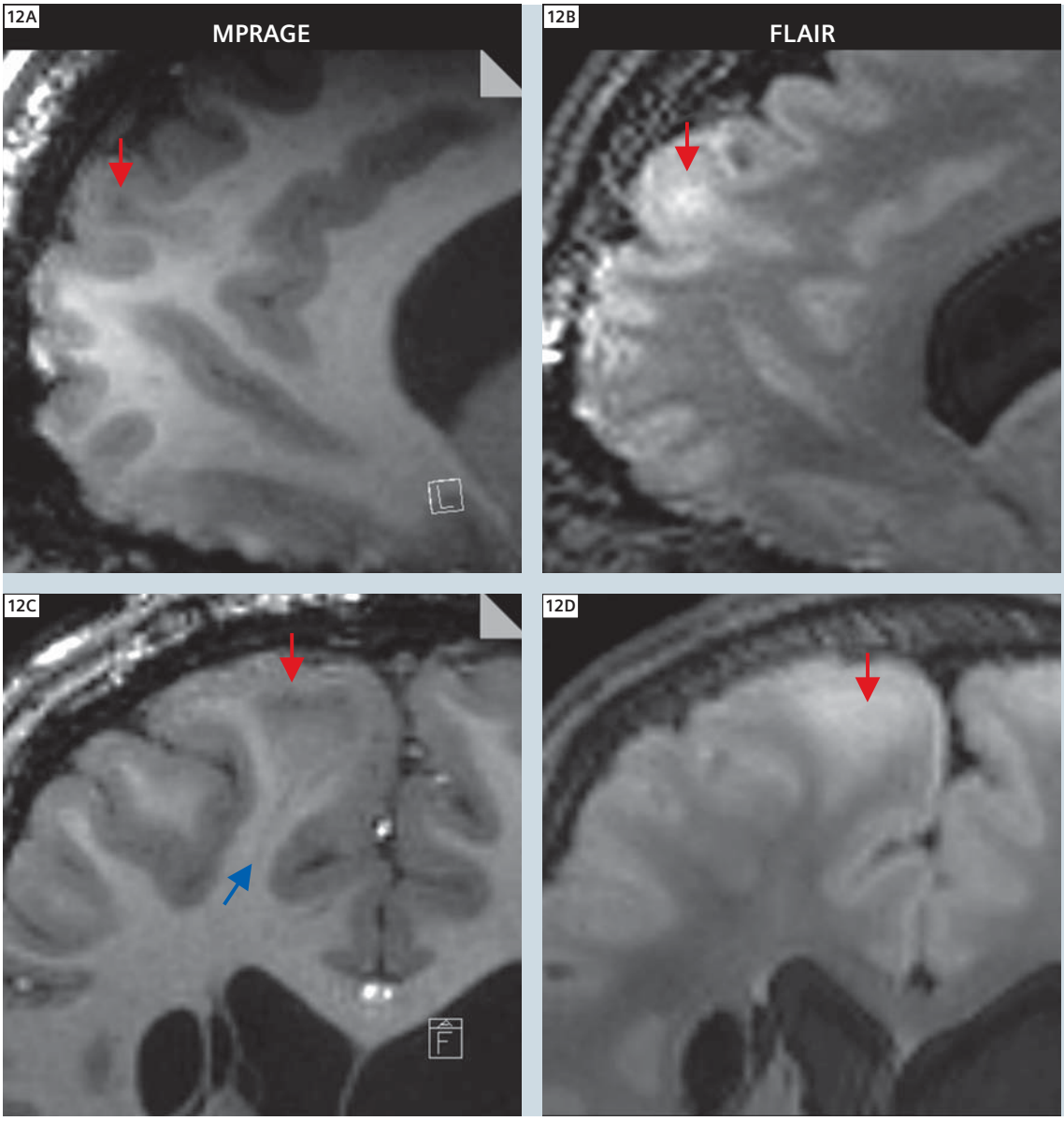

12 Depiction of cortical tuber (red arrows) at 7T with 0.8 mm isotropic MPRAGE (left) and 1 mm isotropic SPACE FLAIR (right). A thin ribbon of grey matter can be seen tracking in towards the ventricle in an axial view (bottom left, blue arrow) – an example of cortical dysplasia. The tuber is hyperintense in the FLAIR images (right). (MPRAGE, 0.8 x 0.8 x 0.8 mm^3, TR/ TE 2250/3.8 ms, TI 1100 ms, acquisition time 5:30 min; SPACE-FLAIR, 1.0 x 1.0 x 1.0 mm^3, TR/ TE 8000/380 ms, TI 2100 ms, 160 partitions, acquisition time 9:39 min. Nova Medical Inc single-element transmit 24-element receive 7T close-fitting brain array.)

Schizophrenia

Another collaboration between the Departments of Psychiatry and Radiology at our institution resulted in the recent publication of 7T images of the human hippocampus *in vivo* [7], with spatial resolution sufficient to visualize directly such small but important structures as the dentate granule cell layer, which is known to be a locus of neural stem cells. Figure 13 extends this work, showing a direct comparison of coronal and sagittal images between a schizophrenic patient and a healthy control. The smooth regular contour of the inferior border of the hippocampus and the well-defined dentate granule cell layer in the healthy subject may be compared to the ridged appearance of the inferior border and general poor visibility of the dentate layer in the patient. Note that the dentate granule cell layer cannot be seen in images taken at lower magnetic field strengths. The use of images such as these is now being contemplated to identify prodromal individuals at risk of developing schizophrenia, in time to initiate preventive treatment before development of chronic life-altering mental illness. Considering the early age of onset of schizophrenia (typically in the late teens to early 20s), prevention has significant social and economic consequences.

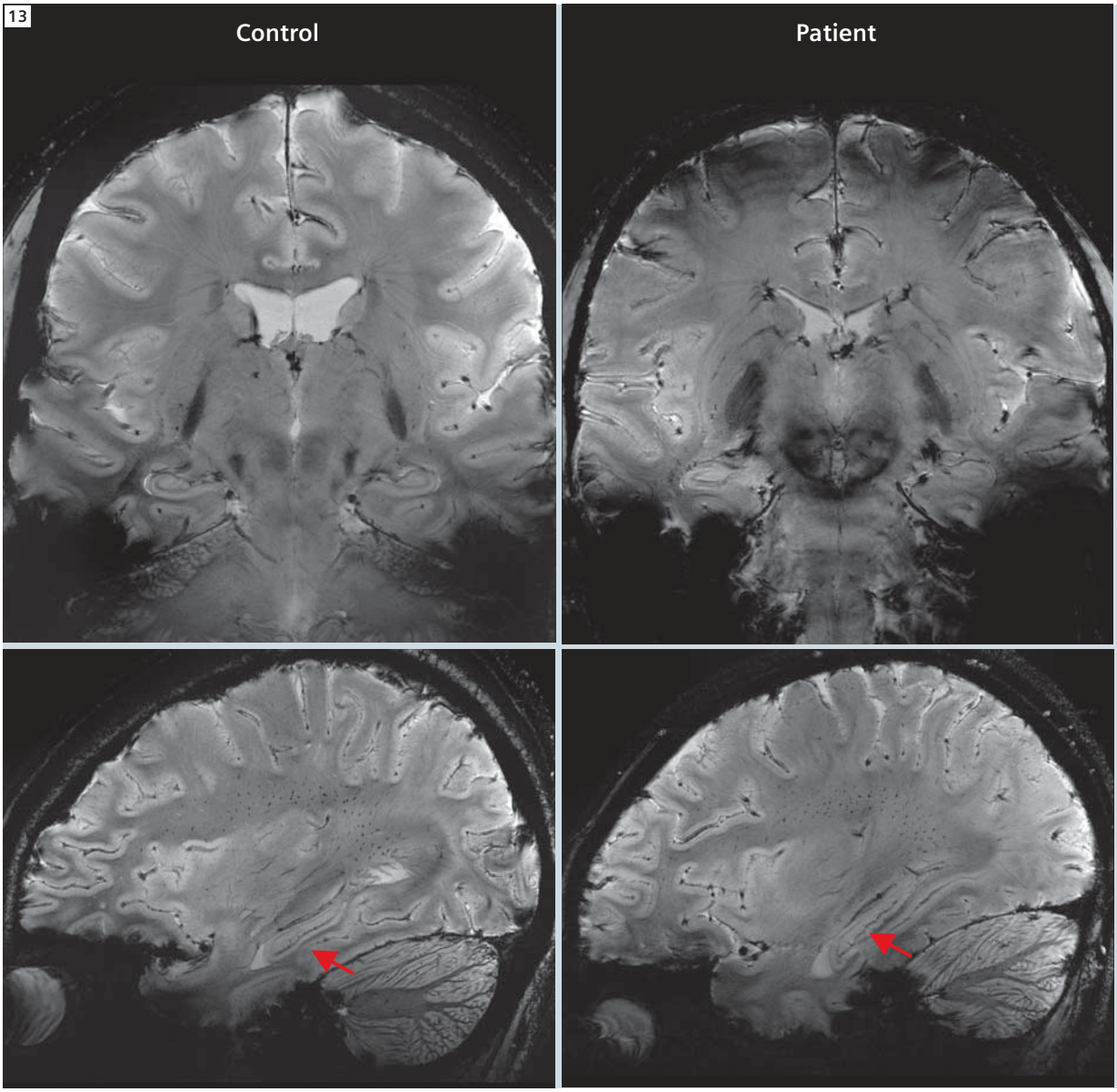

13 T_2*-weighted GRE images of a normal control (left) and a schizophrenic patient (right). Notice the smooth regular contour of the inferior border of the hippocampus and the well-defined dentate granule cell layer in the control, as compared to the ridged appearance of the inferior border and poor visibility of the dentate layer in the patient (arrows). Note also the high contrast in the basal ganglia and in small blood vessels throughout the brain. (T_2*-weighted 2D gradient-echo sequence, TR/TE 944/25 ms, 0.232 × 0.232 ×1.0 mm^3, 17 slices, acquisition time 14:00 min. Nova Medical Inc 24-element 7T head array. *Images courtesy of Oded Gonen, Ph.D., NYULMC, USA.*)

Capturing routine clinical information:

Towards a general purpose clinical 7T neuroimaging protocol

Despite the extraordinary image quality available for selected applications, as evidenced by the examples provided earlier in this article, potential clinical enthusiasm for 7T imaging has been hindered by concerns about its ability to support the range of sequence types and provide the range of image contrasts used for routine clinical evaluations at lower field strengths. In this section, we demonstrate that, with appropriate RF coils and pulse sequence modifications, 7T can in fact provide image quality at least equivalent to that available at 3T for a typical clinical neuroimaging protocol. We have developed a set of protocols at 7T which aim to match or exceed the image quality and coverage of the standard 3T clinical protocol within the same total scan time. This makes it possible to obtain a set of images which correspond closely to familiar 3T scans, but also to take advantage of the unique benefits of 7T through increased resolution or through adding on to the protocol specific scans of interest such as T_2*-weighted GRE, very high resolution MP2RAGE, or Time-of-Flight angiography, obtaining precisely co-registered images in a single scan session. We have chosen certain strategies for optimization of the 7T protocols, but make no claim that these are the optimum sequences for the purpose and offer them primarily as an example and a starting point for others.

While there are particular sequences which routinely produce superior results at 7T than at lower field strength, for maximum diagnostic power the clinician would like to have images of the whole brain in a number of standard contrasts and formats. A typical 3T clinical brain protocol at NYU includes axial T_2-weighted TSE, axial FLAIR, axial T_1-weighted MPRAGE, axial HemoFLASH, axial Diffusion, and possibly also sagittal FLAIR. Imaging with this 3T protocol is typically performed using the standard Siemens 12-channel Matrix head coil. At 7T we use what has become our workhorse 7T head coil array – a single-element transmit, 24-element receive head array from Nova Medical, Inc (the same coil used to obtain the images in Figures 12–13). Note that Nova Medical has also developed a 32-element head array of similar design for use at 7T, and this array is available as part of the Siemens 7T coil portfolio. Both 7T arrays have very close-fitting geometries, which gives them an advantage in SNR compared to the larger Matrix coil, above and beyond the SNR increase due solely to the increased magnetic field strength.

Our image comparisons, therefore, should not be taken as a strict study of field-strength-related behavior, but rather as an investigation into whether we can use available equipment at 7T to match or exceed the accepted clinical standard at 3T. One additional caveat regarding presentation of the images to follow involves image intensity normalization, which we have used in most cases to remove the variation in brightness caused by the sensitivity profiles of the receive array. At lower field strength, the body coil can be used as a relatively uniform reference to determine the bias field, but there is no clear uniform reference at 7T. While there is a 2D normalization filter on the scanner, it is not always able to correct for steep intensity gradients near the receive elements, and it is not appropriate for 3D scans. Therefore, for this article we have processed 7T images with an off-line intensity normalization algorithm provided with the Firevoxel software, a data analysis tool developed by researchers at NYU [8].

For the interested reader, detailed scan parameters for 3T and 7T protocols will be provided in an online supplement to this article (see URL reference at the end). By leveraging the increased SNR at 7T and by carefully calibrating the required transmit power, we can trade off parameters in the various imaging sequences to address issues of inhomogeneity and SAR. To this end, one addition we have made to the standard 3T protocol is an in-house-developed 'B_1 scout,' which uses a nonselective preparation pulse and a TurboFLASH readout to determine what scanner transmitter calibration voltage will produce a 90 degree flip in the center of the head [9]. The standard scanner transmitter calibration routine can provide widely varying estimates of the transmitter calibration voltage, depending on head placement relative to isocenter and other issues. We set the transmitter calibration by hand to an expected value based on previous scans (in this case to 270 volts) and then run our B_1 Scout, which acquires a series of 6 images with different preparation pulses (Fig. 14). The RF voltage for the nominally 90 degree preparation pulse is varied from 80% of the value corresponding to the current transmitter calibration value up to 130% in 10% steps, and the entire series is obtained in 10 seconds. When this series is analyzed with the Mean Curve task card we see that the center of the head reaches a 90 degree flip angle when the transmitter calibration voltage is 270. Looking at the series of B_1 Scout images we can also see that more peripheral regions of the brain do not receive the prescribed excitation even with 130% of the manually entered transmitter calibration voltage. This is the familiar B_1^+ inhomogeneity problem, and we keep this in mind as we optimize our acquisitions during the scan session. After acquisition of localizers and the B_1 scout, the first clinical sequence we run at 7T is a 3D MPRAGE with a sagittal slice prescription (adjusted to match the head orientation as seen in the initial 3-plane localizers). The sagittal orientation and 3D nature of this first scan facilitates slice prescriptions for subsequent scans based on anatomical landmarks in the brain such as the anterior commis-

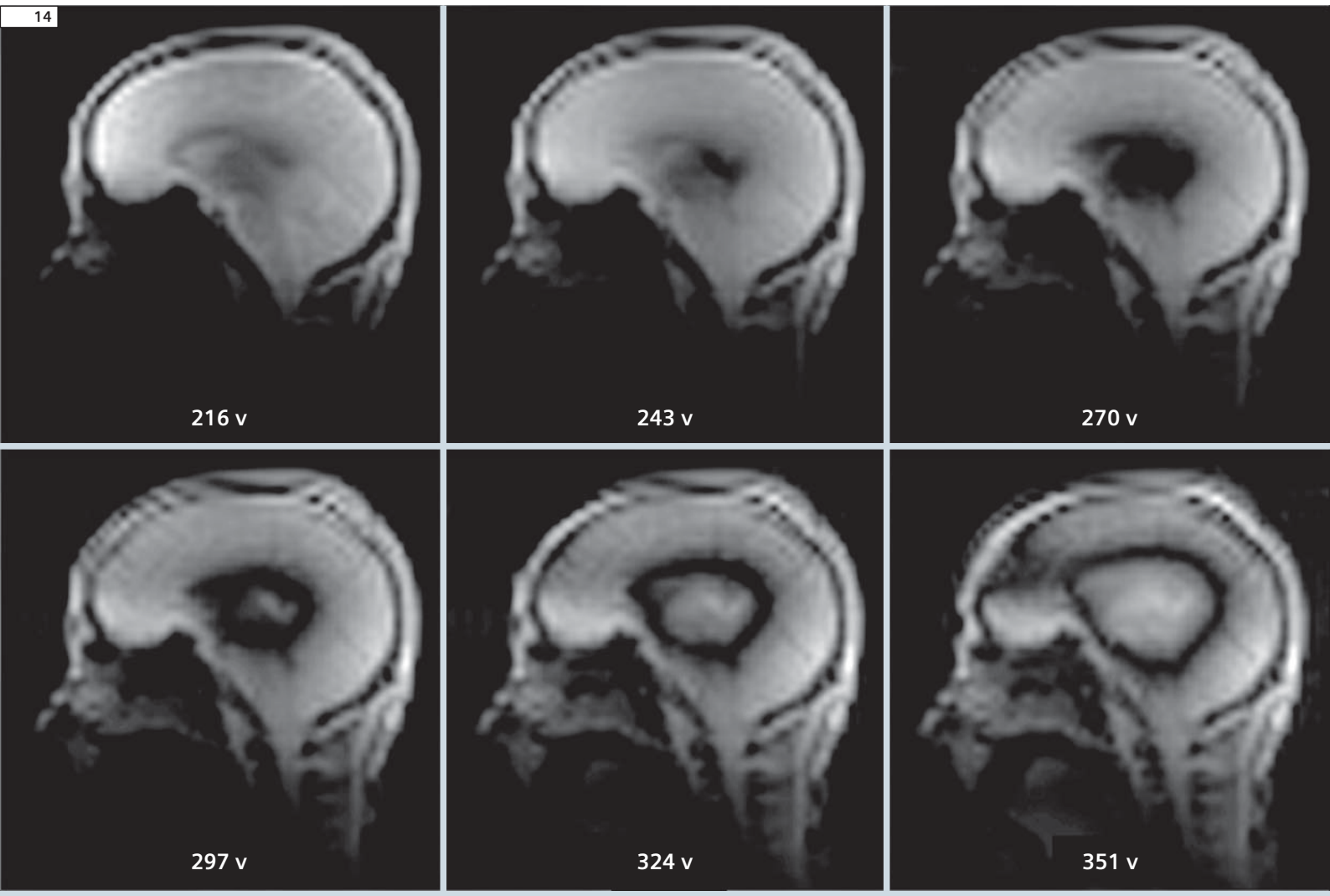

14 In-house-developed 'B_1 Scout', which applies a non-selective preparation pulse of different magnitudes before a TurboFLASH readout. The preparation pulse corresponds to 90 degrees flip at the transmitter reference voltage listed below each image. Black areas represent regions where the preparation pulse achieved a 90 degree excitation. With a transmitter reference of 270 volts we achieve the prescribed flip angle at the center of the head. (TR/TE 2000/1.3 ms, BW 2000, flip angle 8°, 4.7 x 4.7 x 8 mm^3, acquisition time 0:12 min.)

sure – posterior commissure (AC-PC) line. Given that MPRAGE is a low SAR sequence, and that we know the transmitter reference voltage needed to reach the target flip angle in peripheral brain regions is higher than for central regions, we open the adjustments task card before running the scan and set the transmitter reference voltage to 375 for this scan. For comparison to the 3T standard, we reformat the scan into 1 mm thick axial planes, as shown in figure 15. Even with the higher resolution at 7T the SNR clearly exceeds that of the 3T image, and lengthening the inversion time (TI) to 1100 ms maintains good grey-white contrast. The 7T image clearly depicts thin perivascular spaces in the white matter which are lost in the noise in the 3T image. It should be noted, however, that while the MPRAGE sequence produces high quality T_1-weighted images at 7T, there are some issues such as loss of contrast immediately superior to the nasal and auditory sinuses (due to B_0 variation) and in the inferior temporal lobes and inferior cerebellum (due to weak RF transmit field in these regions). These artifacts may be reduced through sequence modifications [10, 11] but we have used the standard ("product") sequence here.

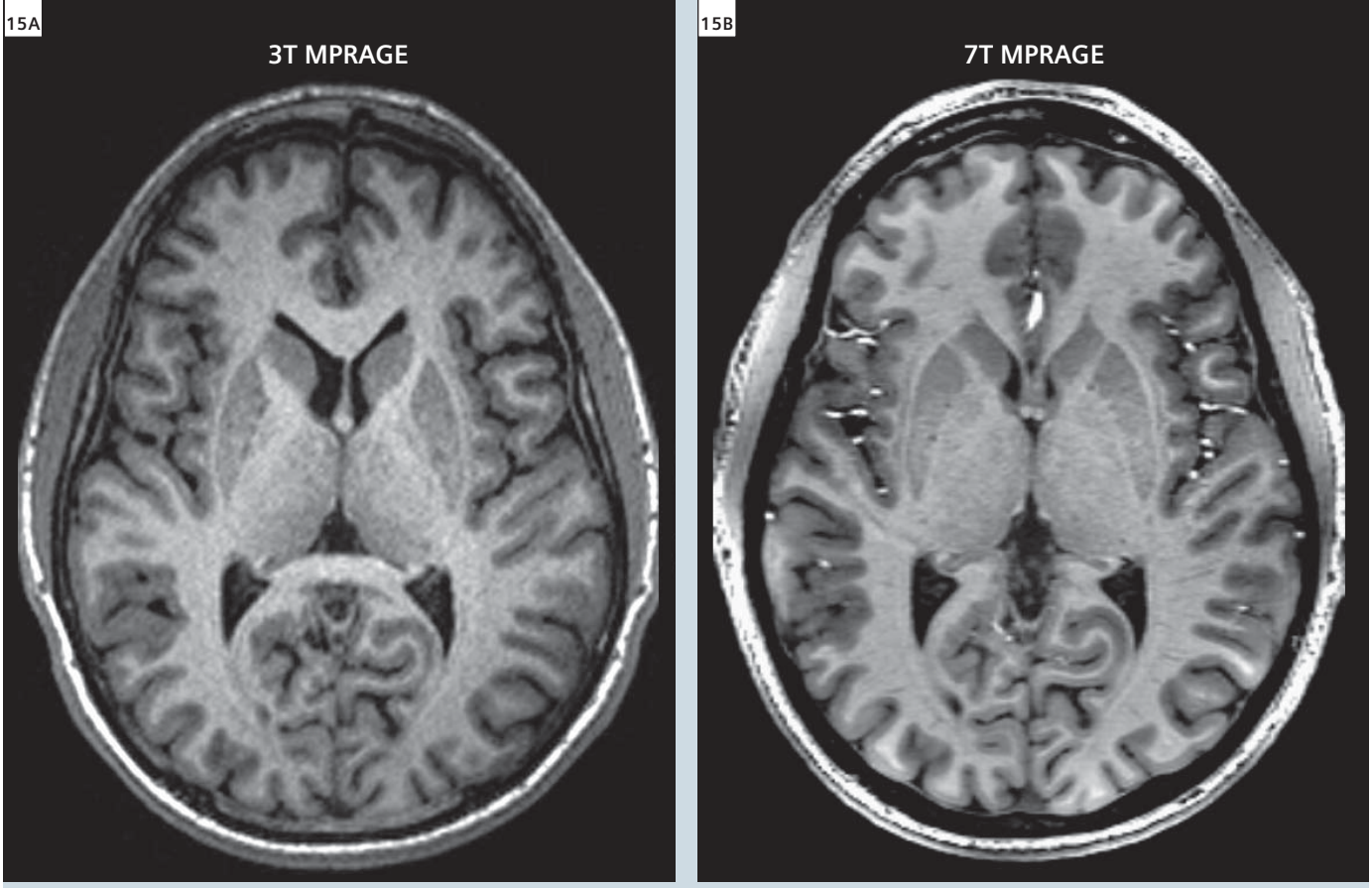

15 Comparison of 3T and 7T MPRAGE scans. Left: 3T, 1.0 x 1.0 x 1.0 mm^3 isotropic resolution, acquisition time 4:31. Right: 7T, reformatted to 0.7 x 1.0 x 1.0 mm^3, acquisition time 4:38.

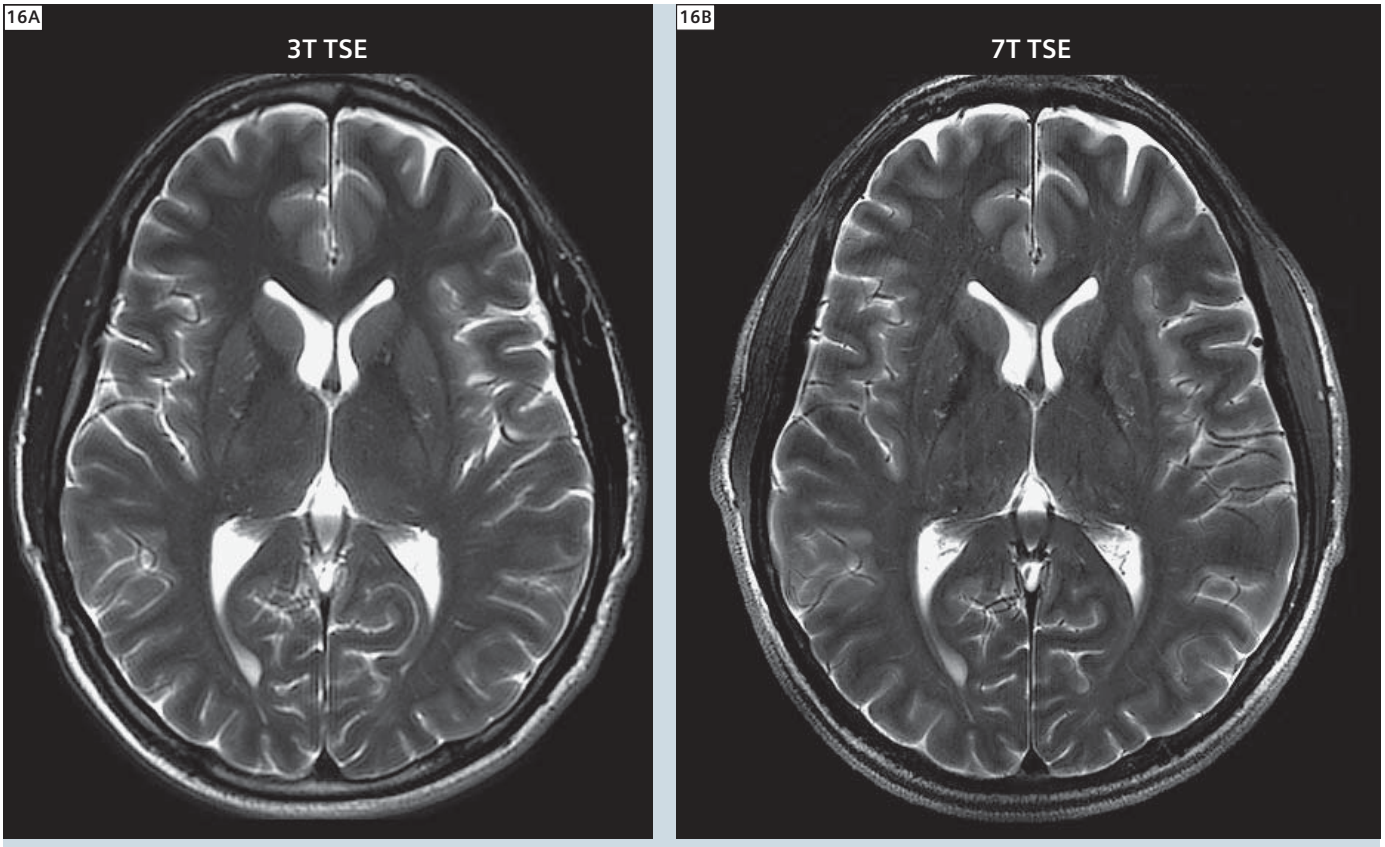

16 Comparison of 3T and 7T TSE images. Left: 3T, 0.7 x 0.7 x 5.0 mm^3, 30 slices, acquisition time 3:16 min. Right: 7T, 0.5 x 0.5 x 3.5 mm, 40 slices, acquisition time 3:06 min.

The next sequence is a T_2-weighted TSE. The TSE sequence is a high SAR sequence due to its series of refocusing pulses. However, thanks to the high SNR provided by our 7T system we can lengthen TR and reduce the field of view, still reaching higher resolution than at 3T within the same total scan time. With regards to the transmitter reference voltage, here our strategy is to use the highest voltage that can be set without triggering the SAR monitor, so that we can get the full number of slices we desire. In this case we set the transmitter reference voltage to 230 volts. The comparison images (Fig. 16, details in Fig. 17) show that we have achieved very similar contrast and superior image quality with the 7T image.

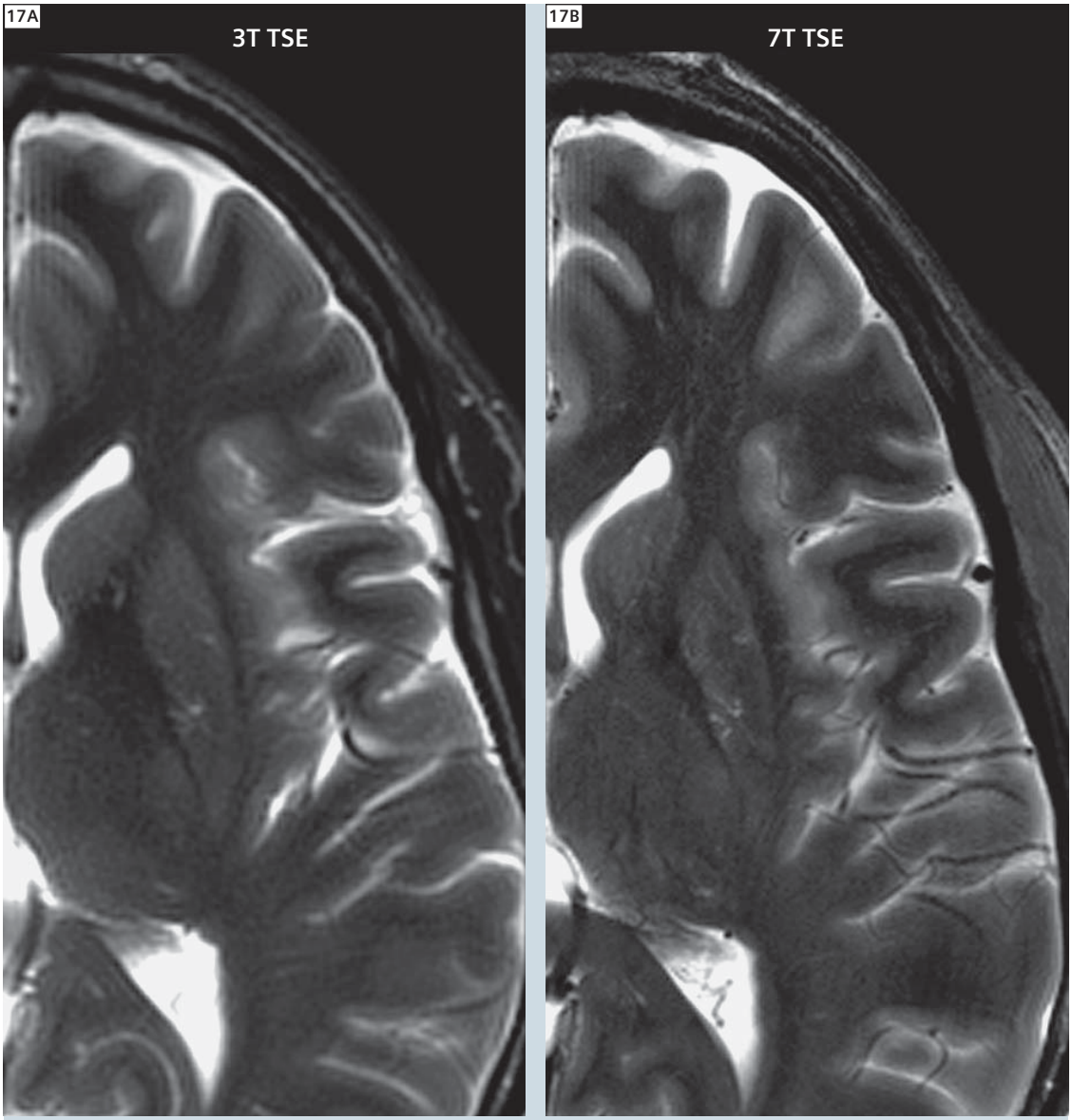

17 Details from images in Figure 16.

Standard FLAIR sequences are difficult to utilize at 7T because their inversion pulse and multiple refocusing pulses result in very high SAR. We have achieved similar image contrast to 3T FLAIR images with 2D sequences, but only with a limited number of slices in the standard scan time due to SAR restrictions. However, a Siemens works in progress (WIP) sequence is available based on the 3D SPACE sequence which provides FLAIR-like contrast. We run this at 1 mm isotropic resolution, and the scan time is roughly equivalent to the combined time taken for axial and sagittal FLAIR scans at 3T. The isotropic 7T data set can then be reformatted into any plane. With this set of parameters we are able to boost the transmitter reference voltage again without exceeding the SAR limits, in this case to 350 volts. We compare 3T images with corresponding 7T reformats in Figures 18–19. There are some differences in the contrast and image quality between the 3T and 7T scans, but with this new sequence we can add FLAIR contrast to our standard protocol at 7T. We have not yet evaluated whether the two approaches yield equivalent diagnostic information about brain lesions, but the 7T SPACE-FLAIR is a powerful addition to the array of sequences which can be run routinely at 7T. HemoFLASH is a 2D FLASH sequence with a relatively long TE to create low signal in regions of high susceptibility, such as where there are blood products from hemorrhage or microbleeds. At 3T a TE of 20 ms is used, with a slice thickness of 5 mm. Given that T_2 in the brain is shorter at 7T than at 3T, we reduce TE to 15 ms, and also reduce the slice thick-

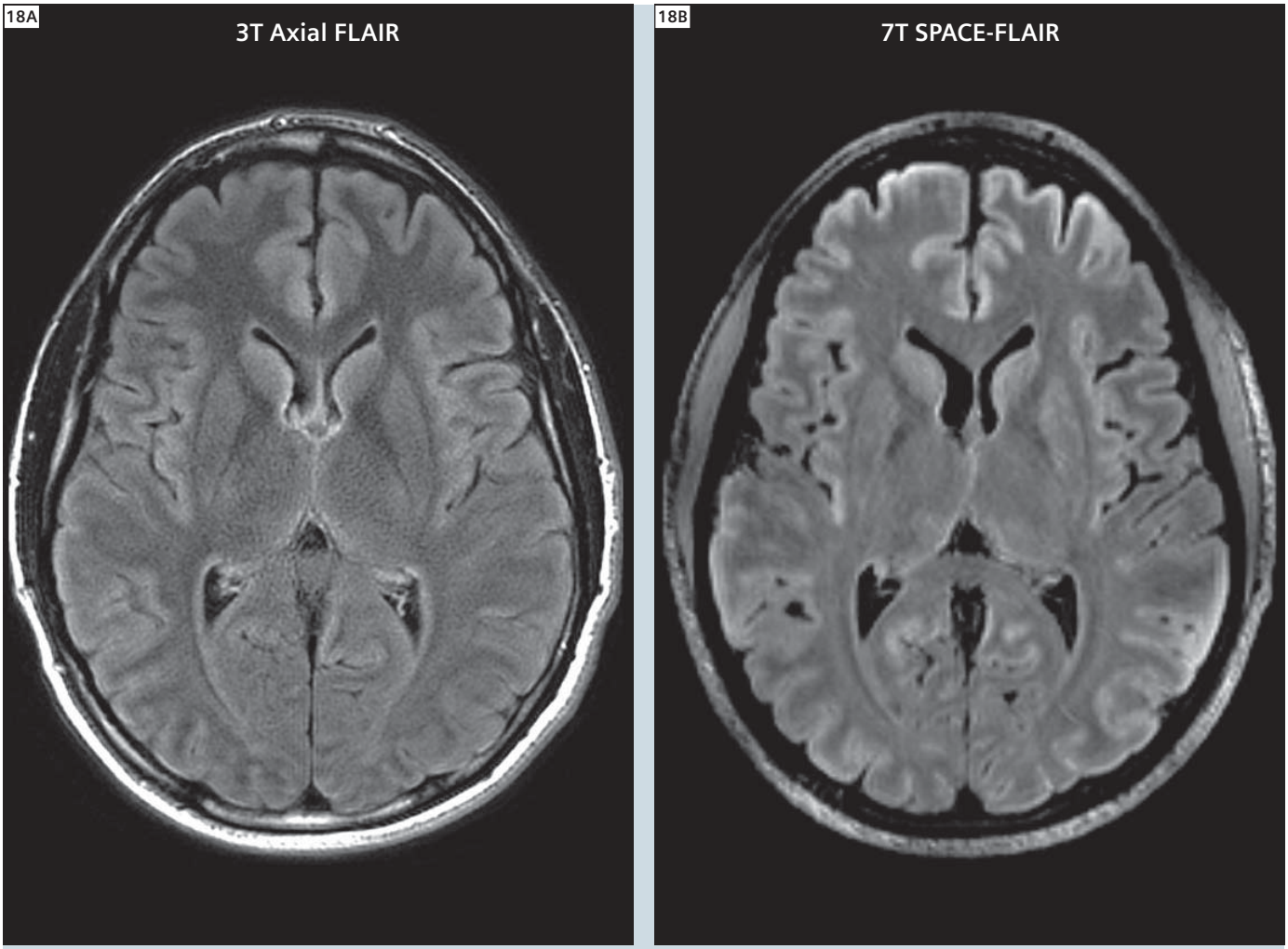

18 Comparison of 3T and 7T FLAIR images. Left: 3T axial FLAIR, 0.7 x 0.7 x 5.0 mm^3, 30 slices, acquisition time 3:02 min. Right: 7T SPACE-FLAIR (3D), 1.0 x 1.0 x 1.0 mm^3, 160 sagittal slices, axial reformat, acquisition time 7:22 min.

ness to 3 mm to reduce signal dropout over the nasal sinus due to through-plane dephasing. Since FLASH is a low SAR sequence, we leave the transmitter reference voltage at 350. We achieved similar image contrast at higher resolution in the same total scan time as compared to 3T (Fig. 20), though there is still some signal dropout over the nasal sinus at this level of the brain. Further sequence optimization might reduce the sensitivity to susceptibility to a level more similar to 3T if desired.

Diffusion-weighted sequences are especially challenging at 7T. They are particularly susceptible to distortions due to B_0 variations, which are larger at 7T than at 3T even with diligent shimming, and the shorter T_2 at 7T leads to loss of signal because of the long readout time. Various strategies can be employed to overcome these issues, such as using higher acceleration rates with parallel imaging, and using thinner slices. We have reduced the matrix size and increased the acceleration compared to the 3T protocol, resulting in a lower in-plane resolution, and have reduced the slice thickness to 3 mm from 5 mm to reduce through-plane dephasing. SAR constraints prevented us from obtaining more than 22 slices with the nominal 270 volt transmitter reference. The 7T diffusion images shown in figure 21 are not of equal quality to those that are routinely obtained at 3T. That said, substantial research efforts have been devoted to diffusion imaging at 7T, and specialized sequences may well be able to achieve improved results [12–15].

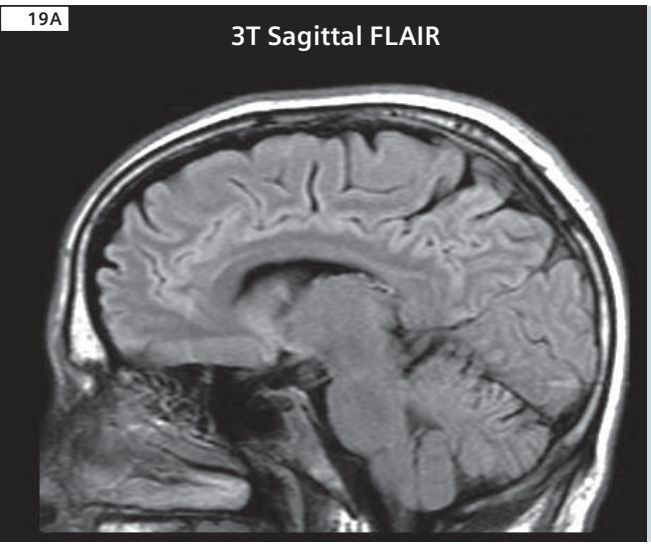

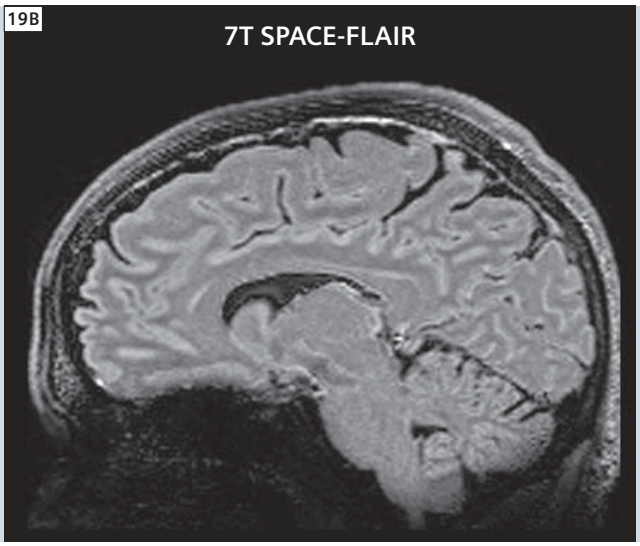

19 Comparison of 3T and 7T FLAIR images. Left: 3T sagittal FLAIR, 1.3 x 0.9 x 5.0 mm³, 30 slices, acquisition time 4:03 min. Right: 7T SPACE-FLAIR (3D), 1.0 x 1.0 x 1.0 mm³, 160 sagittal slices, native sagittal image from the same dataset as for figure 18, acquisition time 7:22 min.

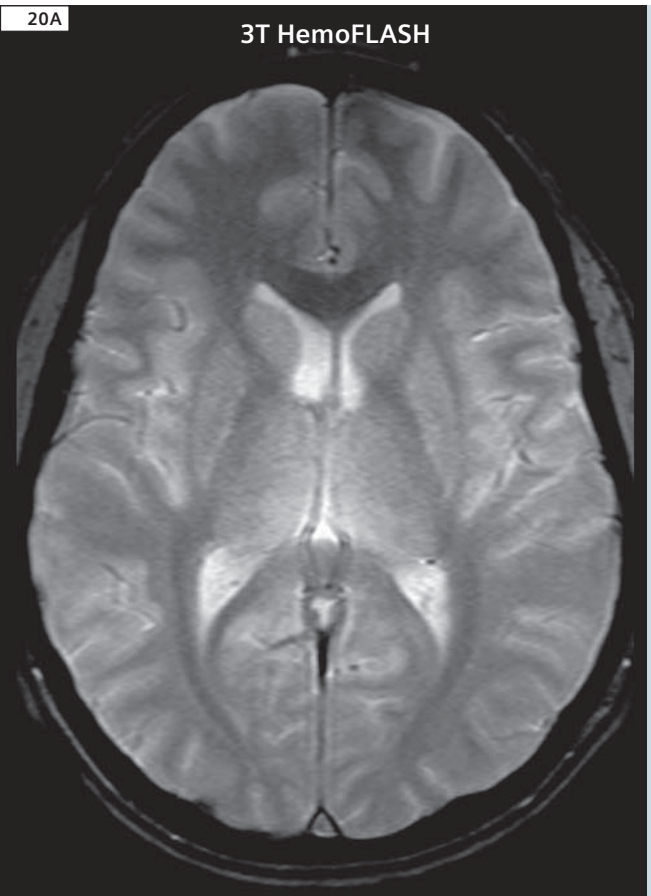

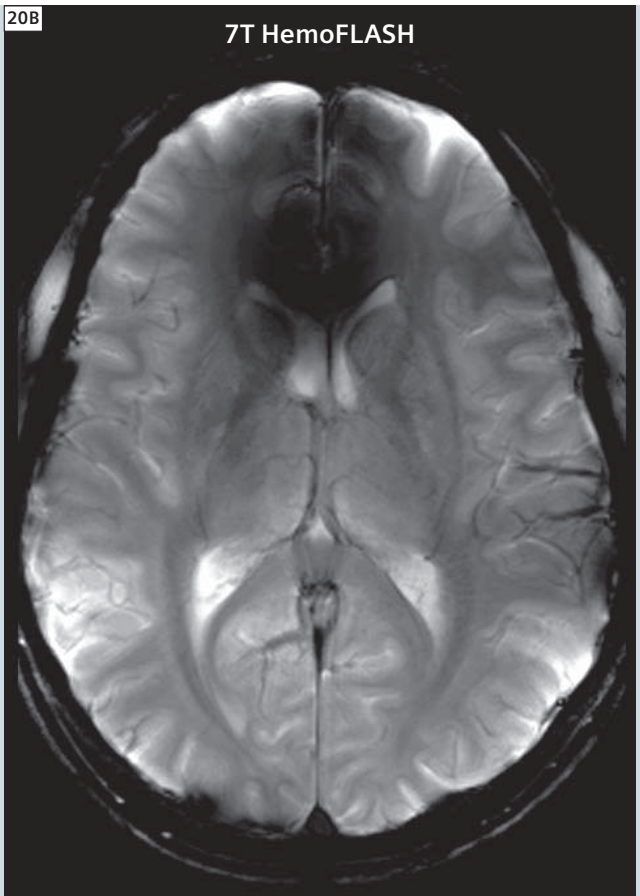

20 Comparison of 3T and 7T HemoFLASH images. Left: 3T, 1.1 x 0.7 x 5.0 mm³, 30 slices, acquisition time 2:35 min. Right: 7T, 0.7 x 0.7 x 3.0 mm³, 45 slices, acquisition time 2:38 min.

In total, not including time spent on localizers, adjustments and slice placement, the 3T protocol occupies 21 minutes 23 seconds, while the 7T protocol requires exactly 22 minutes. In these essentially equivalent times we have produced improved T_1- and T_2-weighted images at higher resolution, comparable FLAIR images, and higher-resolution HemoFLASH images which suffer from greater artifacts near regions of high susceptibility gradient than corresponding 3T images. Only with diffusion imaging do we encounter a real challenge in matching the image quality routinely obtained at 3T, consistent with the general experience that diffusion imaging requires additional optimization at 7T. There are a few caveats for the 7T protocol. To match the imaging time we often used a reduced phase field-of-view, creating a rectangular field-of-view that requires more careful placement and may not provide sufficient coverage for all heads. We have also been unable within the scope of this article to show the entire set of slices covering the whole brain, and there are a few regions in the inferior portion of the brain where susceptibility and RF inhomogeneity artifacts are more pronounced in the 7T images than in the 3T images.
Figure 22 summarizes the results just presented, illustrating graphically the near-equivalence of routine clinical image content at 3T and 7T, combined, of course, with the potential for unique information only at 7T. Note that similar imaging protocol optimizations are likely to be possible for routine musculoskeletal imaging, and further work may bring other body areas to a similar state.

Conclusions

As is evidenced by the images presented here, unique information relevant to various disease processes is currently available at 7T. There has been some hesitation in the past about clinical use of 7T, given concerns about whether traditional clinical information remained available despite changes in contrast, signal inhomogeneity, SAR limitations, etc. Here we demonstrate for a neuroimaging protocol that, with appropriate RF coils, pulse sequence modifications, and imaging protocol optimizations, 7T scanners may be used without losing most of the key clinical information content present in traditional imaging protocols at lower field strengths. This means that unique information of new clinical value may now be accessed without sacrificing routine clinical information. After a period of exploratory development, a portfolio of robust commercially-available coils is now available for 7T use. Availability of self-shielded 7T scanner designs should facilitate incorporation into hospital settings, and ongoing work on 7T body imaging should continue to expand the list of indications for 7T imaging.
In summary, the tool of 7T MRI has been carefully tuned over the past several years. And increasingly, when we are asked the question *'When will 7 Tesla scanners be ready for clinical use?'* we may finally respond: *'Bring on the patients!'*

Acknowlegments

In addition to all of the colleagues who have generously provided images for this article, we would like to thank Dr. Christian Glaser for helpful conversations and consultations. We are also grateful to the Siemens 7T team and particularly to Bernd Stoeckel for his ongoing collaboration, motivation, and support of our 7T work.

Note on online content

Detailed pulse sequence parameters for the images and scanning protocols described in this article may be found at **www.siemens.com/magnetom-world**

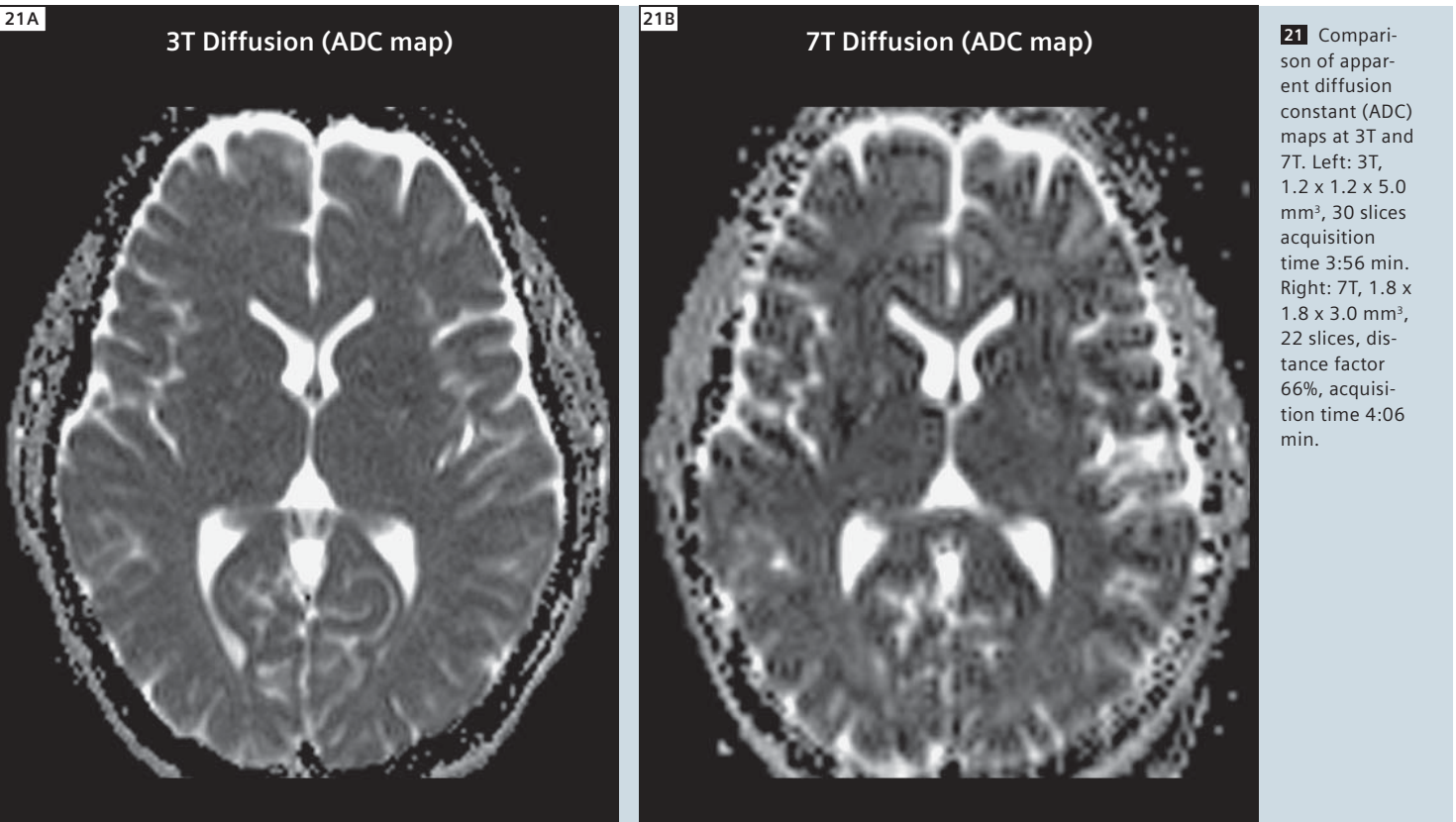

21 Comparison of apparent diffusion constant (ADC) maps at 3T and 7T. Left: 3T, 1.2 x 1.2 x 5.0 mm³, 30 slices acquisition time 3:56 min. Right: 7T, 1.8 x 1.8 x 3.0 mm³, 22 slices, distance factor 66%, acquisition time 4:06 min.

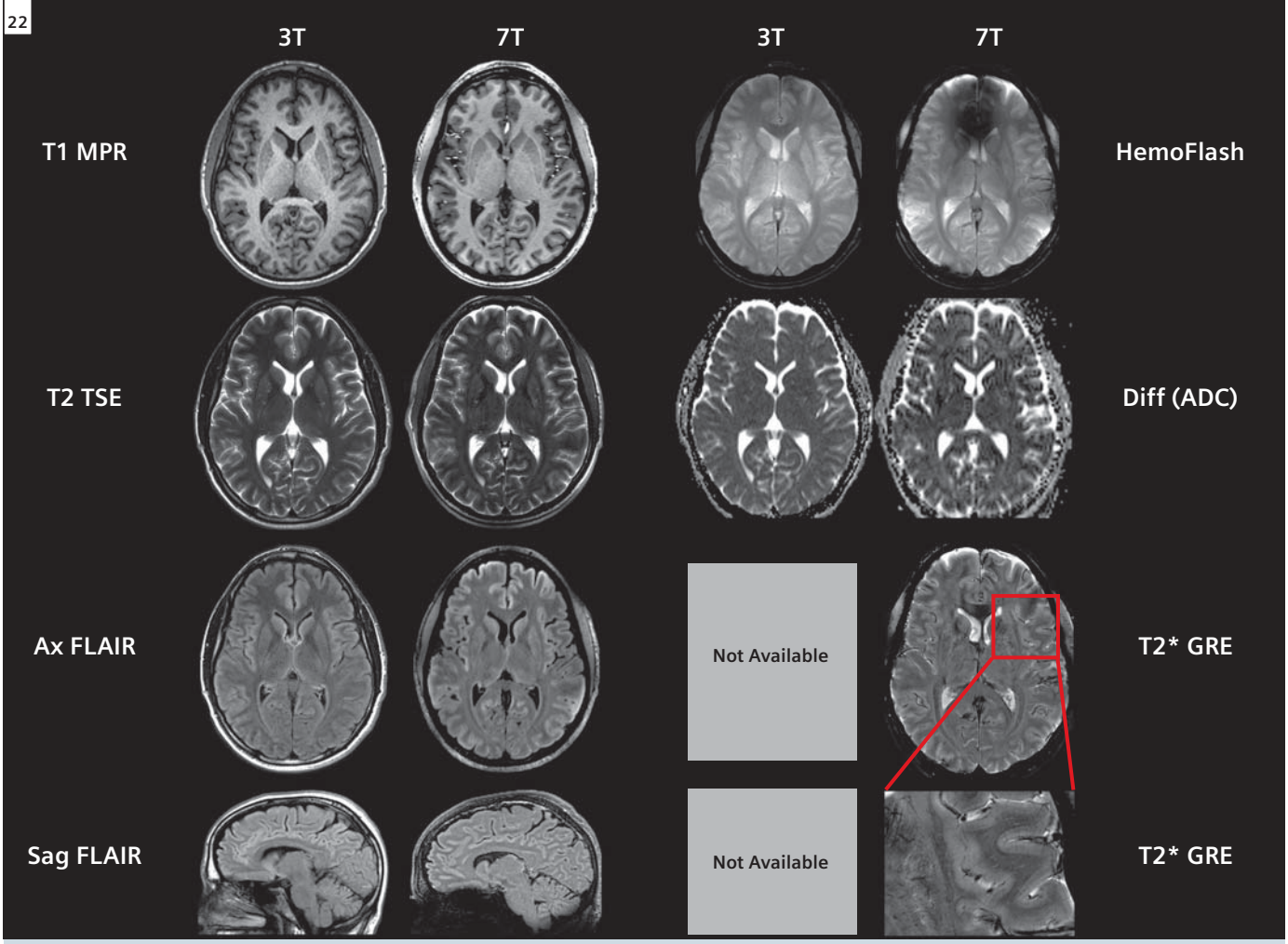

22 Summary of results from 3T and 7T neuroimaging protocols. Images at the bottom right indicate that traditional clinical information, preserved by the 7T protocol, may be supplemented by sequences which provide unique information at 7T.

References

1. Wiggins G, Zhang B, Duan Q, Lattanzi R, Biber S, Stoeckel B, McGorty K, Sodickson D. 7 Tesla Transmit-Receive Array for Carotid Imaging: Simulation and Experiment. Proceedings 17th Scientific Meeting, International Society for Magnetic Resonance in Medicine, 2009:393.
2. Finnerty M, Yang X, Zheng T, et al. A 7-Tesla High Density Transmit with 28-Channel Receive-Only Array Knee Coil. Proceedings 18th Scientific Meeting, International Society for Magnetic Resonance in Medicine. Stockholm, Sweden., 2010:642.
3. Wehrli FW, Song HK, Saha PK, Wright AC. Quantitative MRI for the assessment of bone structure and function. NMR Biomed 2006;19(7):731-64.
4. Chang G, Pakin SK, Schweitzer ME, Saha PK, Regatte RR. Adaptations in trabecular bone microarchitecture in Olympic athletes determined by 7T MRI. J Magn Reson Imaging 2008;27(5):1089-95.
5. Duan Q, Sodickson DK, Lattanzi R, Zhang B, Wiggins G. Optimizing 7T Spine Array Design through Offsetting of Transmit and Receive Elements and Quadrature Excitation. Proceedings 18th Scientific Meeting, International Society for Magnetic Resonance in Medicine. Stockholm, Sweden., 2010:51.
6. Brown R, McGorty K, Moy L, DeGregorio S, Sodickson DK, Wiggins GC. Sub-Millimeter Breast Imaging and Relaxivity Characterization at 7T. Proceedings 19th Scientific Meeting, International Society for Magnetic Resonance in Medicine. Montreal, CA, 2011:3092.
7. Prudent V, Kumar A, Liu S, Wiggins G, Malaspina D, Gonen O. Human hippocampal subfields in young adults at 7.0 T: feasibility of imaging. Radiology;254(3):900-6.
8. Mikheev A, Nevsky G, Govindan S, Grossman R, Rusinek H. Fully automatic segmentation of the brain from T1-weighted MRI using Bridge Burner algorithm. J Magn Reson Imaging 2008;27:1235-1241 (https://files.nyu.edu/hr18/public/projects.html).
9. Chung S, Kim D, Breton E, Axel L. Rapid B_1^+ mapping using a preconditioning RF pulse with TurboFLASH readout. Magn Reson Med 2010;64(2):439-46.
10. Wiggins C. A Simple Method Of Improving MPRAGE Inversion Coverage at 7T. Proceedings 15th Scientific Meeting, International Society for Magnetic Resonance in Medicine. Seattle, WA, USA, 2007:3448.
11. Marques JP, Kober T, Krueger G, W. van der Zwang W, Van de Moortele P-F, Gruetter R. MP2RAGE contrast optimization at 7T and applications. Proceedings 17th Scientific Meeting, International Society for Magnetic Resonance in Medicine. Honolulu, HI, USA, 2009:2698.
12. Mukherjee P, Hess CP, Xu D, Han ET, Kelley DA, Vigneron DB. Development and initial evaluation of 7-T q-ball imaging of the human brain. Magn Reson Imaging 2008;26(2):171-80.
13. Heidemann RM, Porter DA, Anwander A, Feiweier T, Heberlein K, Knosche TR, Turner R. Diffusion imaging in humans at 7T using readout-segmented EPI and GRAPPA. Magn Reson Med 2010;64(1):9-14.
14. von Morze C, Kelley DA, Shepherd TM, Banerjee S, Xu D, Hess CP. Reduced field-of-view diffusion-weighted imaging of the brain at 7 T. Magn Reson Imaging 2010;28(10):1541-5.
15. Sigmund EE, Gutman D. Diffusion-weighted Imaging of the Brain at 7 T with Echo-planar and Turbo Spin Echo Sequences: Preliminary Results. Magnetic Resonance Imaging 2011:in press.

Contact
Daniel K. Sodickson, MD, PhD
Vice-Chair for Research, Department of Radiology
Director, Center for Biomedical Imaging
New York University Langone Medical Center
660 First Avenue, Fourth Floor
New York, NY 10016
USA
Phone: +1 212-263-4844
Daniel.Sodickson@med.nyu.edu